Rapid Communications

Incommensurate two-dimensional checkerboard charge density wave in the low-dimensional superconductor $Ta_4Pd_3Te_{16}$

Zhenzhong Shi [1], S. J. Kuhn,[1] F. Flicker,[2] T. Helm [3,4] J. Lee [5] William Steinhardt,[1] Sachith Dissanayake,[1] D. Graf,[6] J. Ruff,[5] G. Fabbris,[7] D. Haskel [7] and S. Haravifard[1,8,*]

[1]*Department of Physics, Duke University, Durham, North Carolina 27708, USA*
[2]*Rudolph Peierls Centre for Theoretical Physics, University of Oxford, Department of Physics, Clarendon Laboratory, Parks Road, Oxford OX1 3PU, United Kingdom*
[3]*Max Planck Institute for Chemical Physics of Solids, 01187 Dresden, Germany*
[4]*Dresden High Magnetic Field Laboratory (HLD-EMFL), Helmholtz-Zentrum Dresden-Rossendorf, 01328 Dresden, Germany*
[5]*Cornell High Energy Synchrotron Source, Cornell University, Ithaca, New York 14853, USA*
[6]*National High Magnetic Field Laboratory, Florida State University, Tallahassee, Florida 32310, USA*
[7]*Advanced Photon Source, Argonne National Laboratory, Argonne, Illinois 60439, USA*
[8]*Department of Mechanical Engineering and Materials Science, Duke University, Durham, North Carolina 27708, USA*

We report the observation of a two-dimensional (2D) checkerboard charge density wave (CDW) in the low-dimensional superconductor $Ta_4Pd_3Te_{16}$. By determining its CDW properties across the temperature-pressure (T-P) phase diagram and comparing with prototypical CDW materials, we conclude that $Ta_4Pd_3Te_{16}$ features (a) an incommensurate CDW with a mixed character of dimensions [quasi-1D (Q1D) considering its needlelike shape along the b axis, Q2D as the CDW has checkerboard wave vectors, and 3D because of CDW projections along all three axes], and (b) one of the weakest CDWs compared to its superconductivity (SC), i.e., enhanced SC with respect to CDW, suggesting an interesting interplay of the two orders.

Charge density waves (CDWs), electronic instabilities originally considered in one dimension (1D) [1], have now been found in various forms and exist not only in quasi-one-dimensional (Q1D) materials but also in quasi-two-dimensional (Q2D) and three-dimensional (3D) systems [2,3]. Q1D systems such as the transition metal trichalcogenide compounds are generally expected to be unstable to CDW formation via the Peierls instability, i.e., Fermi-surface (FS) nesting (FSN) [4]. However, in systems with higher dimensions, such as the transition metal dichalcogenides (Q2D) and cubic system $R_3T_4X_{13}$ (3D) [5,6], FSN is not the natural explanation for CDW formation. A single wave vector will always nest the two points of the FS onto one another in 1D; in 2D and 3D a special shape of FS would be required to match large portions of the FS onto itself. Instead, CDWs in higher-dimensional materials such as $NbSe_2$, often have a more complex origin involving the momentum and orbital dependence of the electron-phonon coupling matrix [7–9].

The electron-phonon coupling required for the CDW order may also facilitate superconductivity (SC) based on the standard Bardeen-Cooper-Schrieffer (BCS) mechanism [10],

and the two orders are often found to be proximal or to co-exist [2,3,11–15]. However, the interplay of the CDW and SC may extend well beyond the BCS picture, where the pairing mechanism may not be phonon mediated and the SC becomes unconventional. In cuprates, for example, the relative strength of the SC with respect to the charge order is much stronger than that in conventional superconductors [13] and the interplay of charge order and SC is still highly debated [16–20]. It is possible that SC in some unconventional superconductors could be enhanced by quantum fluctuations accompanied by the suppression of the CDW to a quantum critical point (QCP) [21,22]. In reality, however, it is extremely difficult to discern the different yet possibly intertwined mechanisms contributing to the interplay of the CDW and SC, including dimensionality and critical fluctuations. Here, we report a CDW system that may serve as an ideal platform for such studies.

Featuring three chains of $PdTe_2$, $TaTe_3$, and Ta_2Te_4 along its b axis, aligned into planes perpendicular to c, the monoclinic crystalline structure of $Ta_4Pd_3Te_{16}$ with lattice parameters $a = 17.687$ Å, $b = 3.735$ Å, $c = 19.510$ Å, and $\beta = 110.42°$ [23] is reminiscent of those of trichalcogenide compounds such as $ZrSe_3$, $TaSe_3$, $NbSe_3$, and TaS_3. However, transport measurements on $Ta_4Pd_3Te_{16}$ indicate resistivity ratios along the $\mathbf{a^*} : \mathbf{b} : \mathbf{c}$ directions of $4 : 1 : 13$ at room temperature (T), evolving to $10 : 1 : 20$ just above the superconducting transition $T_c \sim 4.6$ K [24]. The ratios suggest a rather weak anisotropy, and the material itself is better thought of as having a character of mixed dimension-

---

*Corresponding author: sara.haravifard@duke.edu

ality: Q1D (along b), Q2D (cleavage plane perpendicular to c), and 3D (relatively weak anisotropy), which, as we will show below, underlies an interesting 2D checkerboard CDW in this system with wave vectors projected along all three axes.

Previous studies of $Ta_4Pd_3Te_{16}$ have revealed an anisotropic SC ground state [25,26]. Under pressure (P), a dome-shaped SC phase with maximum $T_c \sim 6$ K at 0.2–0.3 GPa was discovered [27,28]. Some evidence suggests that the SC order parameter in $Ta_4Pd_3Te_{16}$ might have a d-wave symmetry and thus an unconventional origin [25,27,29]. Others have argued that the experimental findings may be explained by the more conventional s-wave SC order parameter and the multiband nature of the compound [30–32]. While phase-sensitive measurements are needed to eventually reveal the pairing symmetry, the SC in $Ta_4Pd_3Te_{16}$ is also interesting because of hints of its proximity to a CDW phase [24,30–33]. NMR/NQR [31] and thermodynamic measurements [24] suggest a CDW transition temperature (T_{CDW}) of ~20 K, while Raman scattering measurements support the emergence of CDW fluctuations below 140–200 K [33]. Additionally, scanning tunneling microscopy (STM) measurements have shown period-4 commensurate CDW-like stripes along the b axis that coexist with SC [30]. However, the suggested wave vector is seemingly at odds with transport measurements, which reveal a resistivity anomaly primarily along the a^* direction while being much weaker along the b and c directions [24]. Therefore, a direct measurement of the bulk CDW in $Ta_4Pd_3Te_{16}$ is critical for reconciling these experimental results and understanding the interplay of SC and CDW in this material.

In this Rapid Communication, we report the direct observation of a delicate CDW in $Ta_4Pd_3Te_{16}$ using synchrotron x-ray diffraction (see Supplemental Material [34]). We establish the T-P phase diagram, which reveals a low $T_{CDW} \sim 16$ K at ambient P, quickly suppressed with increasing P, becoming undetectable where T_c reaches its maximum. Our de Haas–van Alphen (dHvA) oscillation measurements (see Fig. S2 and related text in Supplemental Material [34]) do not show any sign of FS reconstruction through the CDW transition, consistent with an earlier report [24]. The observed CDW has a checkerboard pattern in real space, which resembles more closely the checkerboard CDW in quasi-2D systems such as $NbSe_2$ [3] rather than those in typical Q1D systems such as $NbSe_3$, where multiple CDWs, if they exist, are typically unidirectional and independent [2]. However, unlike the CDWs seen in most Q2D systems, the CDW in $Ta_4Pd_3Te_{16}$ does not lie within the Q2D planes. These peculiar dimensional properties may explain its weak CDW, as we discuss in detail below.

We obtained the most direct evidence of a checkerboard CDW in $Ta_4Pd_3Te_{16}$ using ambient-P x-ray diffraction [34], which provides an unambiguous identification of the bulk CDW and its wave vectors. Using a high-dynamic-range area detector, we scanned wide areas across multiple Brillouin zones in many directions, including along the wave vector [0 0.25 0] suggested by a previous STM study [30]. However, our x-ray scans did not reveal any CDW peak along this direction. Instead, we identified two peaks at wave vectors **Q1** = [−0.2 0.21 −0.3] and **Q2** = [0.2 0.21 0.3] in all the
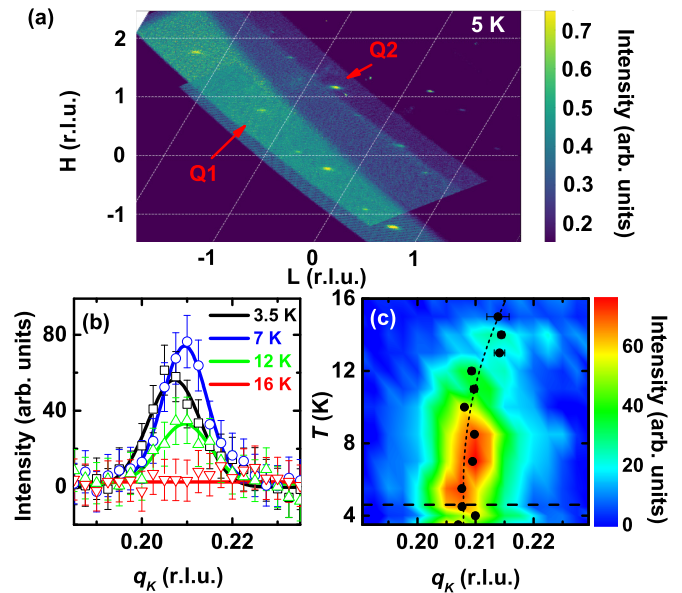

FIG. 1. (a) 2D diffraction pattern along H and L at $K = 4.21$ for $T = 5$ K, where H, K, and L positions are given in reciprocal lattice units (r.l.u.). Two CDW peaks, labeled as Q1 and Q2, appear in all the Brillouin zones covered in the experiment: **Q1** $\sim$ $(-0.20, 0.21, -0.30)$ and **Q2** $\sim (0.20, 0.21, 0.30)$. The same observation is made at $K = 2.21$. (b) The CDW peak $[(-1, 4, 1) + (-0.20, q_k, -0.30)]$ Q1 along K for several T, with the 30-K background trace subtracted. Solid lines are Lorentzian fits to data. Error bars correspond to 1 standard deviation (SD) (square root of number of counts). (c) Contour plot of the background-subtracted Q1 CDW intensity along K. Black data points indicate the peak centers of Lorentzian fits at each T. The short-dashed line guides the eye. The horizontal dashed line indicates $T_c = 4.6$ K [23].

Brillouin zones within our detection range [Fig. 1(a)]. The integrated intensity of the CDW peak is $\sim 10^{-3}$ the strength of that at the nearby Bragg peak. The **Q1** and **Q2** wave vectors are related by a $180°$ rotation about the b axis. Together they constitute a commensurate pattern of the superlattice along the H and L (or a^* and c^*) directions.

We repeated the measurements at different T from 3.5 K up to 30 K. Figure 1(b) shows the line cuts and their Lorentzian fits along the K direction for the Q1 CDW near the $(-1\ 4\ 1)$ Bragg peak for a few selected T. The entire set of data consisting of the line cuts at all measured T is summarized in a color contour plot in Fig. 1(c). It is clear that, with T increasing from 3.5 K, the Q1 CDW peak intensity first increases and plateaus at 5–9 K, then diminishes and becomes undetectable at $T_{CDW} \sim 16$ K, and this is accompanied by a slight shift in the peak position. Our results are consistent with the $T_{CDW} \sim 20$ K inferred from NMR/NQR [31] and transport measurements [24]. We do not see any evidence of a static CDW above ~16 K, though our measurements cannot rule out the possibility of fluctuating CDW order at higher T. The signatures of phonon anomalies at higher T [33] therefore might be attributed to a pseudogap phase, similar to that in $NbSe_2$ [35]. A comparison between T_{CDW} (~16 K) and the energy gap ($\Delta = 20$–30 meV) observed by STM [30] suggests that the CDW in $Ta_4Pd_3Te_{16}$ is in the strong-coupling
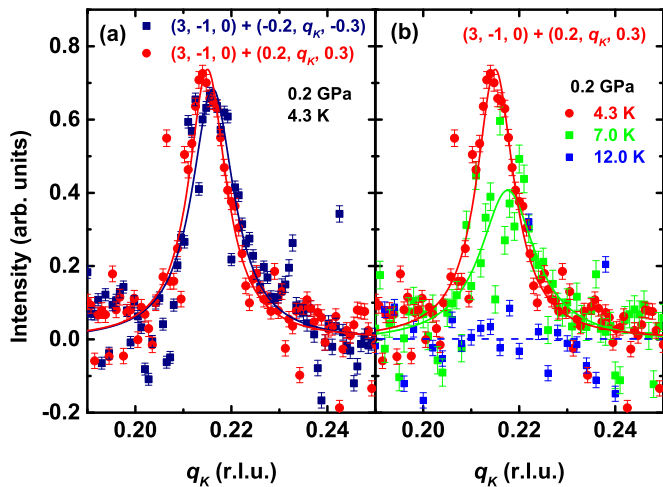
FIG. 2. (a) The projected Q1 and Q2 CDW peak profiles along K near $(3, -1, 0)$ at $T = 4.3$ K and $P = 0.2$ GPa. (b) The T dependence of the projected Q2 CDW peak profile at $P = 0.2$ GPa. A linear background is subtracted from all the data. Solid lines are Lorentzian fits to the data. The dashed line is a guide to the eye. Error bars correspond to 1 SD.

FIG. 3. The T dependence of (a) the normalized peak intensity, (b) the peak position, and (c) the FWHM along q_k for the Q1 CDW at 0 GPa and Q2 CDW at 0.2 GPa. The peak intensity shown in (a) is normalized to its value at 4.5 K for ambient P and its value at 4.3 K for 0.2 GPa. Solid lines guide the eye. Black and red dashed lines indicate T_c at ambient P and 0.2 GPa [23,28]. (d) T-P phase diagram of $Ta_4Pd_3Te_{16}$. The open red symbol at 0.35 GPa is a null data point, where no CDW peak is seen [34]. The phase boundary of the incommensurate CDW (ICDW) phase, determined by the two data points at 0 and 0.2 GPa as well as the null data point at 0.35 GPa, is also indicated in the Fig. 4 by the red dashed line. T_c values are from Ref. [27].

limit ($3.52 k_B T_c \ll 2\Delta$), again similar to the case in $NbSe_2$ [9] and cuprates [13]. It is interesting to point out that our observation is consistent with an early band structure study on rare-earth tellurides which suggests that a checkerboard state would occur with sufficiently low T_{CDW}, while a unidirectional (stripe) CDW is favored with higher T_{CDW} [36].

To confirm our observations at ambient P, and to further explore the T-P phase diagram, we also conducted x-ray diffraction under pressure at a different synchrotron source [34]. With the lowest pressure achieved in our measurement ($P = 0.2$ GPa [34]), we again observed the Q1 and Q2 CDWs near the $(3 - 1\,0)$ Bragg peak, at $T = 4.3$ K, as shown in Fig. 2(a). The ratio of the integrated intensity of the CDW peak and the nearby Bragg peak is again $\sim 10^{-3}$, in good agreement with our ambient-P results. The intensities of the two CDWs are comparable within error, consistent with the picture of one checkerboard CDW. The T dependence of the q_k line cuts are measured for the Q2 CDW at $P = 0.2$ GPa. The results as seen in Fig. 2(b) clearly show that the peak intensity is quickly suppressed with increasing T, and becomes undetectable at 12 K. Moreover, as shown in Fig. S4, our experiments do not show any sign of CDW [34] at higher P (0.35 GPa), where the peak position of the reported SC dome resides [27,28]. Therefore, we find that the CDW becomes weaker, characterized by a smaller T_{CDW}, with increased P, and disappears at higher P when the SC is strongest (maximum T_c). This seems to suggest a competitive nature of the interplay between CDW and SC, and is consistent with the fact that the ambient-P CDW peak intensity plateaus at 9–5 K, below which the SC emerges and CDW peak intensity is weakened [see Figs. 1(c) and 3(a)]. However, as discussed below, we do not rule out the effect of quantum fluctuations near a CDW QCP on the SC. In cuprates, for example, while a reduced CDW intensity below T_c was reported as evidence for a CDW competing with SC [37], a recent study also revealed the importance of a charge order quantum critical point [21].
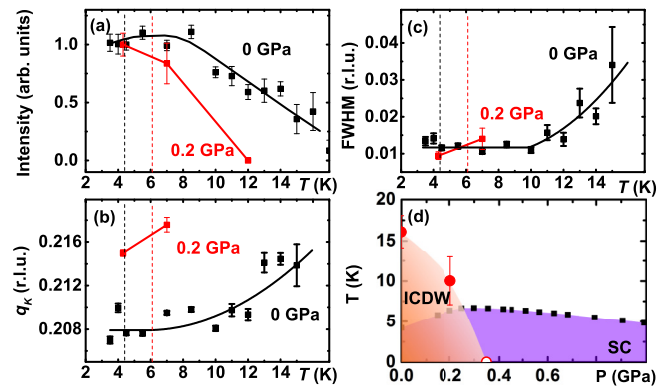
The T dependence of the CDW peak position along q_k, as shown in Figs. 1(c) and 3(b), shows some unexpected behaviors. At ambient P the CDW peak center along q_k shifts towards a commensurate value 0.2 (a real-space periodicity of 5) with decreasing T, but saturates before locking into that value. The peak also shifts further away from $q_k = 0.2$ under pressure. Therefore, it appears that the CDW remains incommensurate along q_k down to the lowest T. Typically, one expects the CDW wave vector to evolve continuously with T until abruptly jumping to a commensurate value, in a first-order lock-in phase transition [38]. Examples include Q1D tetrathiafulvalene-tetracyanoquinodimethane (TTF-TCNQ) and Q2D $TaSe_2$. However, many other materials show an evolution of the CDW wave vector without an eventual lock-in [2], such as Q1D $NbSe_3$ and $TbTe_3$ and Q2D $NbSe_2$. Our observations indicate that $Ta_4Pd_3Te_{16}$ falls into this latter category.

The CDW wave vectors, $\mathbf{Q1} = [-0.2\ 0.21\ -0.3]$ and $\mathbf{Q2} = [0.2\ 0.21\ 0.3]$, featuring modulations along all three axes, appear at first to be at odds with the CDW reported in the previous STM study, which found a period-4 commensurate charge modulation only along the b axis [30]. This discrepancy underlies the importance of the synchrotron x-ray measurement in directly observing the bulk CDW, in contrast to the STM, which is sensitive only to the projection of the charge modulation onto the sample surface [i.e., the $(-1\ 0\ 3)$ cleavage plane]. A careful analysis of the $\mathbf{Q1}$ and $\mathbf{Q2}$ wave vectors and their projections on different planes (see Fig. S3 and the associated discussions in Supplemental Material [34]) confirms that the $\mathbf{Q1}$ and $\mathbf{Q2}$ wave vectors revealed in our x-ray data actually reconciles the apparently conflicting results from STM [30] and transport measurements [24].

The CDW correlation length can be extracted from the width of the CDW peak, which is measured by the full width at half maximum (FWHM) of the Lorentzian fits [Figs. 1(b) and 2, and also see Supplemental Material [34] for more details]. The T-dependent FWHM at $P = 0$ and 0.2 GPa are plotted in Fig. 3(c). At low T, FWHM ~ 0.01 r.l.u., suggesting a CDW correlation length $\xi_{CDW} \sim 120$ Å along q_k [34]. A slight increase of FWHM to 0.015 r.l.u. is seen below T_c, suggesting a possible competitive interplay of CDW with SC. Near T_{CDW} the FWHM increases drastically, and the inferred ξ_{CDW} reduces to ~ 30 Å, which is close to the CDW wavelength (i.e., CDW modulation period) along the b axis $\lambda_b \sim 5b \sim 20$ Å, signaling the melting of the static CDW at higher T.

In Fig. 3(d) we establish the T-P phase diagram using $T_{CDW}(P)$ from our x-ray diffraction measurements and T_c from Ref. [27]. The SC dome peaks at the pressure where the CDW vanishes. Although such observations may generally be expected within standard BCS theory (i.e., T_c increases as the density of states released upon CDW gap closure becomes available for the formation of Cooper pairs), we note that other scenarios including SC related to a CDW QCP [22] may not be ruled out: (a) The energy scales of the CDW and SC are comparable, while the former is typically much larger than the latter in conventional superconductors; and (b) the CDW transition in $Ta_4Pd_3Te_{16}$ appears to be a second-order phase transition, as hinted by the very weak kinklike feature in resistivity [24] and the smooth evolution of the CDW order parameter seen in our x-ray data, although we do not have evidence regarding whether the transition remains second order or sufficiently weak first order at $T = 0$.

Our results reveal a delicate checkerboard CDW in $Ta_4Pd_3Te_{16}$ (see the Supplemental Material [34]). It is found that $Ta_4Pd_3Te_{16}$ features (a) a character of mixed dimensionality, (b) two CDWs related by a lattice symmetry developing at the same T, (c) CDW wavev ectors that are commensurate along two lattice directions but incommensurate along the third even at low T, (d) no clear signatures of FS reconstruction as the CDW develops (see our dHvA oscillation results), and (e) an interesting interplay of the CDW and SC. The uniqueness of the CDW in $Ta_4Pd_3Te_{16}$ is further demonstrated when comparing to other CDW materials.

On the one hand, $Ta_4Pd_3Te_{16}$ is often considered Q1D, structurally similar to the transition metal trichalcogenides such as $NbSe_3$, NbS_3, $ZrSe_3$, and $TaSe_3$, each of which has a monoclinic phase formed from chains within planes, and also the rare-earth tritellurides RTe_3 (R = Sm, Gd, Tb, Dy, Ho, Er, Tm) with weakly orthorhombic structures. All these materials host multiple CDWs [2], which, unlike $Ta_4Pd_3Te_{16}$, are not related by a lattice symmetry, and develop at different T (also see Supplemental Material [34]). On the other hand, the resistivity ratios of $Ta_4Pd_3Te_{16}$ suggest that the material is better thought of not as Q1D but as a dimensional hybrid with Q1D chains within Q2D planes within a 3D material. Density functional theory (DFT) calculations confirm the existence of FS pockets of each dimensionality [32]. Thus a fairer comparison might be found with Q2D CDW materials such as the transition metal dichalcogenides (TMDC) $2H$-$NbSe_2$, $2H$-$TaSe_2$, and $1T$-TaS_2 [38,39], which, however, feature CDW entirely within the Q2D planes.
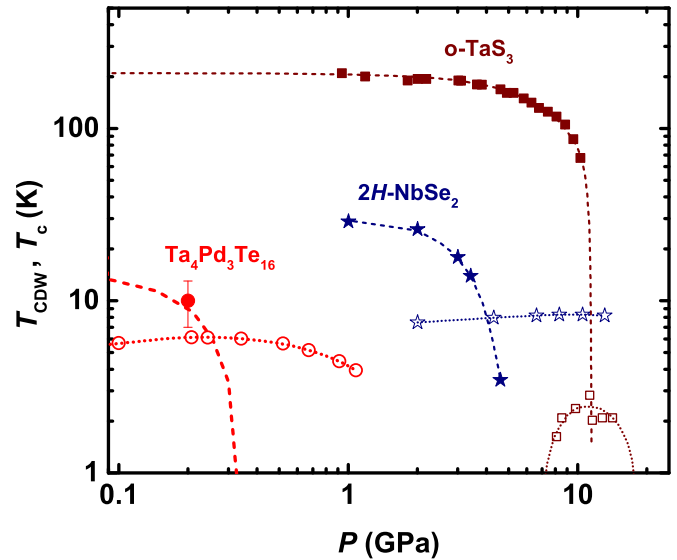

FIG. 4. Phase diagram of a few selected compounds, as a function of T and P, showing T_{CDW} (solid symbols) and T_c (open symbols). For $Ta_4Pd_3Te_{16}$, the CDW phase boundary, determined from our x-ray data at 0, 0.2, and 0.35 GPa and indicated by the red dashed line, is shown along with T_c values from Ref. [28]. Note that logarithmic scales are used for both axes due to the vastly different scales for the different materials. As a result, our data points at $P = 0$ and $T_{CDW} \sim 0$ become invisible, though the red dashed line remains as a good indicator for the CDW phase boundary. Other compounds: $2H$-$NbSe_2$ [38,43]; o-TaS_3 [41,42].

It has previously been argued that CDWs never truly develop by a Q1D Peierls-type mechanism [7–9]. From this point of view, all compounds with a purported low-dimensional character might more reasonably be thought of as dimensional hybrids, with $Ta_4Pd_3Te_{16}$ simply being a particularly clear example. A consequence can be seen in the behavior of the CDW under pressure, and its interaction with SC. As noted in Ref. [2], increasing P has the effect of increasing interchain (or interplane) coupling, which might have one of two opposite effects on T_{CDW} depending on how Q1D the system really is. In extreme Q1D systems, T_{CDW} is heavily suppressed by fluctuations to well below the value predicted by mean-field theory [40]. The reduction in interchain spacing (increased interchain coupling) decreases the one-dimensional character of the system, suppressing these fluctuations, and increasing T_{CDW}. On the other hand, if T_{CDW} is not dictated by Q1D fluctuations, the primary effect of the increased interchain coupling is to decrease the density of states at the Fermi level, suppressing T_{CDW}. In the standard BCS picture, the phonon mode formerly suppressed by the CDW could become available to mediate SC at high P and an SC phase could develop, although the resulting SC phase does not necessarily form a dome centered around the vanishing of the CDW. As shown in Figs. 4 and S5, such a picture seems to apply to many Q2D and 3D materials [e.g., $2H$-$NbSe_2$ [43], $2H$-TaS_2 [44,45], $1T$-TaS_2 [46], $1T$-$TaSe_2$ [47], $1T$-$TiSe_2$ [48], $(Ca, Sr)_3Ir_4Sn_{13}$ [5,6]] (see Supplemental Material [34]), as well as to $Ta_4Pd_3Te_{16}$ to a certain extent. However, as explained above, we do not rule out the en-

hancement of T_c due to possible QCP-related fluctuations in $Ta_4Pd_3Te_{16}$ and the possibility of an incommensurate density wave quantum criticality in 2D metals has recently been discussed [49].

In summary, we report a direct observation of a bulk CDW with its checkerboard wave vectors in $Ta_4Pd_3Te_{16}$. It shows several interesting characteristics: (a) a unique mixed character of dimensionality and (b) the lowest value of the T_{CDW}/T_c among prototypical CDW materials. Future studies with probes sensitive to both CDW and SC [e.g., high-P Raman spectroscopy, angle-resolved photoemission spectroscopy (ARPES), second harmonic generation, etc.] are desirable in order to fully understand this interesting interplay.

[1] R. Peierls, *Quantum Theory of Solids* (Oxford University Press, London, 1955).

[2] P. Monceau, Electronic crystals: An experimental overview, Adv. Phys. **61**, 325 (2012).

[3] C.-W. Chen, J. Choe, and E. Morosan, Charge density waves in strongly correlated electron systems, Rep. Prog. Phys. **79**, 084505 (2016).

[4] G. Grüner, The dynamics of charge-density waves, Rev. Mod. Phys. **60**, 1129 (1988).

[5] L. E. Klintberg, S. K. Goh, P. L. Alireza, P. J. Saines, D. A. Tompsett, P. W. Logg, J. Yang, B. Chen, K. Yoshimura, and F. M. Grosche, Pressure- and Composition-Induced Structural Quantum Phase Transition in the Cubic Superconductor (Sr, Ca)$_3$Ir$_4$Sn$_{13}$, Phys. Rev. Lett. **109**, 237008 (2012).

[6] S. K. Goh, L. E. Klintberg, P. L. Alireza, D. A. Tompsett, J. Yang, B. Chen, K. Yoshimura, and F. M. Grosche, Enhancement of the superconducting transition temperature with hydrostatic pressure in Ca$_3$Ir$_4$Sn$_{13}$ single crystals, arXiv:1105.3941.

[7] M. D. Johannes and I. I. Mazin, Fermi surface nesting and the origin of charge density waves in metals, Phys. Rev. B **77**, 165135 (2008).

[8] X. Zhu, Y. Cao, J. Zhang, E. W. Plummer, and J. Guo, Classification of charge density waves based on their nature, Proc. Natl. Acad. Sci. USA **112**, 2367 (2015).

[9] F. Flicker and J. van Wezel, Charge order from orbital-dependent coupling evidenced by NbSe$_2$, Nat. Commun. **6**, 7034 (2015).

[10] J. Bardeen, L. N. Cooper, and J. R. Schrieffer, Microscopic theory of superconductivity, Phys. Rev. **106**, 162 (1957).

[11] T. Wu, H. Mayaffre, S. Krämer, M. Horvatić, C. Berthier, W. N. Hardy, R. Liang, D. A. Bonn, and M.-H. Julien, Magnetic-field-induced charge-stripe order in the high-temperature superconductor YBa$_2$Cu$_3$O$_y$, Nat. Commun. **477**, 191 (2011).

[12] T. Wu, H. Mayaffre, S. Krämer, M. Horvatić, C. Berthier, W. N. Hardy, R. Liang, D. A. Bonn, and M.-H. Julien, Incipient charge order observed by NMR in the normal state of YBa$_2$Cu$_3$O$_y$, Nat. Commun. **6**, 6438 (2015).

[13] R. Comin and A. Damascelli, Resonant x-ray scattering studies of charge order in cuprates, Annu. Rev. Condens. Matter Phys. **7**, 369 (2016).

[14] D. E. Moncton, J. D. Axe, and F. J. DiSalvo, Study of Superlattice Formation in $2H$-NbSe$_2$ and $2H$-TaSe$_2$ by Neutron Scattering, Phys. Rev. Lett. **34**, 734 (1975).

[15] P. Monceau, N. P. Ong, A. M. Portis, A. Meerschaut, and J. Rouxel, Electric Field Breakdown of Charge-Density-Wave-Induced Anomalies in NbSe$_3$, Phys. Rev. Lett. **37**, 602 (1976).

[16] A. M. Gabovich, A. I. Voitenko, and M. Ausloos, Charge- and spin-density waves in existing superconductors: Competition between Cooper pairing and Peierls or excitonic instabilities, Phys. Rep. **367**, 583 (2002).

[17] M. R. Norman, The challenge of unconventional superconductivity, Science **332**, 196 (2011).

[18] E. Fradkin, S. A. Kivelson, and J. M. Tranquada, Colloquium: Theory of intertwined orders in high temperature superconductors, Rev. Mod. Phys. **87**, 457 (2015).

[19] Z. Shi, P. G. Baity, T. Sasagawa, and D. Popović, Vortex phase diagram and the normal state of cuprates with charge and spin orders, Sci. Adv. **6**, eaay8946 (2020).

[20] Z. Shi, P. G. Baity, J. Terzic, T. Sasagawa, and D. Popović, Pair density wave at high magnetic fields in cuprates with charge and spin orders, Nat. Commun. **11**, 3323 (2020).

[21] W. S. Lee *et al.*, Spectroscopic fingerprint of charge order melting driven by quantum fluctuations in a cuprate, Nat. Phys. (2020), doi: 10.1038/s41567-020-0993-7.

[22] T. Gruner, D. Jang, Z. Huesges, R. Cardoso-Gil, G. H. Fecher, M. M. Koza, O. Stockert, A. P. Mackenzie, M. Brando, and C. Geibel, Charge density wave quantum critical point with strong enhancement of superconductivity, Nat. Phys. **13**, 967 (2017).

[23] W.-H. Jiao, Z. T. Tang, Y. L. Sun, Y. Liu, Q. Tao, C.-M. Feng, Y.-W. Zeng, Z.-A. Xu, and G.-H. Cao, Superconductivity in a layered $Ta_4Pd_3Te_{16}$ with $PdTe_2$ chains, J. Am. Chem. Soc. **136**, 1284 (2014).

[24] T. Helm *et al.*, Thermodynamic anomaly above the superconducting critical temperature in the quasi-one-dimensional superconductor $Ta_4Pd_3Te_{16}$, Phys. Rev. B **95**, 075121 (2017).

[25] Z. Du, D. Fang, Z. Wang, Y. Li, G. Du, H. Yang, X. Zhu, and H.-H. Wen, Anisotropic superconducting gap and elongated vortices with Caroli-De Gennes-Matricon states in the new superconductor $Ta_4Pd_3Te_{16}$, Sci. Rep. **5**, 9408 (2015).

[26] W.-H. Jiao, L.-P. He, Y. Liu, X.-F. Xu, Y.-K. Li, C.-H. Zhang, N. Zhou, Z.-A. Xu, S.-Y. Li, and G.-H. Cao, Superconductivity in $Ta_3Pd_3Te_{14}$ with quasi-one-dimensional $PdTe_3$ chains, Sci. Rep. **6**, 21628 (2016).

[27] J. Pan, W. H. Jiao, X. C. Hong, Z. Zhang, L. P. He, P. L. Cai, J. Zhang, G. H. Cao, and S. Y. Li, Nodal superconductivity and superconducting dome in the layered superconductor $Ta_4Pd_3Te_{16}$, Phys. Rev. B **92**, 180505(R) (2015).

[28] N. H. Jo, L. Xiang, U. S. Kaluarachchi, M. Masters, K. Neilson, S. S. Downing, P. C. Canfield, and S. L. Bud'ko, Pressure induced change in the electronic state of $Ta_4Pd_3Te_{16}$, Phys. Rev. B **95**, 134516 (2017).

[29] G. Pang, M. Smidman, W. Jiao, L. Jiao, Z. Wang, W. Jiang, C. Guo, Y. Chen, G. Cao, and H. Yuan, Evidence for nodal superconductivity in a layered compound $Ta_4Pd_3Te_{16}$, J. Phys.: Condens. Matter **30**, 055701 (2018).

[30] Q. Fan *et al.*, Scanning tunneling microscopy study of superconductivity, magnetic vortices, and possible charge-density wave in $Ta_4Pd_3Te_{16}$, Phys. Rev. B **91**, 104506 (2015).

[31] Z. Li, W. H. Jiao, G. H. Cao, and G.-q. Zheng, Charge fluctuations and nodeless superconductivity in quasi-one-dimensional $Ta_4Pd_3Te_{16}$ revealed by ^{125}Te-NMR and ^{181}Ta-NQR, Phys. Rev. B **94**, 174511 (2016).

[32] D. J. Singh, Multiband superconductivity of $Ta_4Pd_3Te_{16}$ from Te *p* states, Phys. Rev. B **90**, 144501 (2014).

[33] D. Chen, P. Richard, Z. D. Song, W. L. Zhang, S. F. Wu, W. H. Jiao, Z. Fang, G. H. Cao, and H. Ding, Raman scattering investigation of the quasi-one-dimensional superconductor $Ta_4Pd_3Te_{16}$, J. Phys.: Condens. Matter **27**, 495701 (2015).

[34] See Supplemental Material at http://link.aps.org/supplemental/10.1103/PhysRevResearch.2.042042 for details on experimental methods, dHvA quantum oscillation results, the CDW in $Ta_4Pd_3Te_{16}$, and additional discussions on CDWs in prototypical CDW materials.

[35] S. V. Borisenko *et al.*, Pseudogap and Charge Density Waves in Two Dimensions, Phys. Rev. Lett. **100**, 196402 (2008).

[36] H. Yao, J. A. Robertson, E.-A. Kim, and S. A. Kivelson, Theory of stripes in quasi-two-dimensional rare-earth tellurides, Phys. Rev. B **74**, 245126 (2006).

[37] J. Chang *et al.*, Direct observation of competition between superconductivity and charge density wave order in $YBa_2Cu_3O_{6.67}$, Nat. Phys. **8**, 871 (2012).

[38] Y. Feng, J. van Wezel, J. Wang, F. Flicker, D. M. Silevitch, P. B. Littlewood, and T. F. Rosenbaum, Itinerant density wave instabilities at classical and quantum critical points, Nat. Phys. **11**, 865 (2015).

[39] B. Giambattista, C. Slough, W. McNairy, and R. Coleman, Scanning tunneling microscopy of atoms and charge-density waves in 1*T*-TaS$_2$, 1*T*-TaSe$_2$, and 1*T*-VSe$_2$, Phys. Rev. B **41**, 10082 (1990).

[40] P. A. Lee, T. M. Rice, and P. W. Anderson, Fluctuation Effects at a Peierls Transition, Phys. Rev. Lett. **31**, 462 (1973).

[41] M. Núñez-Regueiro, J.-M. Mignot, and D. Castello, Superconductivity at High Pressure in NbSe$_3$, Europhys. Lett. **18**, 53 (1992).

[42] M. Núñez-Regueiro, J.-M. Mignot, M. Jaime, D. Castello, and P. Monceau, Superconductivity under pressure in linear chalcogenides, Synth. Met. **56**, 2653 (1993).

[43] M. Leroux, I. Errea, M. Le Tacon, S.-M. Souliou, G. Garbarino, L. Cario, A. Bosak, F. Mauri, M. Calandra, and P. Rodière, Strong anharmonicity induces quantum melting of charge density wave in 2*H*-NbSe$_2$ under pressure, Phys. Rev. B **92**, 140303(R) (2015).

[44] R. Grasset, Y. Gallais, A. Sacuto, M. Cazayous, S. Mañas-Valero, E. Coronado, and M.-A. Méasson, Pressure-Induced Collapse of the Charge Density Wave and Higgs Mode Visibility in 2*H*-TaS$_2$, Phys. Rev. Lett. **122**, 127001 (2019).

[45] D. C. Freitas *et al.*, Strong enhancement of superconductivity at high pressures within the charge-density-wave states of 2*H*-TaS$_2$ and 2*H*-TaSe$_2$, Phys. Rev. B **93**, 184512 (2016).

[46] B. Sipos, A. F. Kusmartseva, A. Akrap, H. Berger, L. Forr, and E. Tutis, From Mott state to superconductivity in 1*T*-TaS$_2$, Nat. Mater. **7**, 960 (2008).

[47] B. Wang, Y. Liu, K. Ishigaki, K. Matsubayashi, J. Cheng, W. Lu, Y. Sun, and Y. Uwatoko, Pressure-induced bulk superconductivity in a layered transition-metal dichalcogenide 1*T*-tantalum selenium, Phys. Rev. B **95**, 220501(R) (2017).

[48] A. F. Kusmartseva, B. Sipos, H. Berger, L. Forró, and E. Tutič, Pressure Induced Superconductivity in Pristine 1*T*-TiSe$_2$, Phys. Rev. Lett. **103**, 236401 (2009).

[49] J. Halbinger, D. Pimenov, and M. Punk, Incommensurate $2k_F$ density wave quantum criticality in two-dimensional metals, Phys. Rev. B **99**, 195102 (2019).

Zhenzhong Shi,[1] S. J. Kuhn,[1] F. Flicker,[2] T. Helm,[3] J. Lee,[4] William Steinhardt,[1]
Sachith Dissanayake,[1] D. Graf,[5] J. Ruff,[4] G. Fabbris,[6] D. Haskel,[6] and S. Haravifard[1]

[1]*Department of Physics, Duke University, Durham, NC 27708, USA*
[2]*Rudolph Peierls Centre for Theoretical Physics, University of Oxford,*
Department of Physics, Clarendon Laboratory, Parks Road, Oxford OX1 3PU, UK
[3]*Max Planck Institute for Chemical Physics of Solids, Dresden, Germany*
[4]*Cornell High Energy Synchrotron Source, Cornell University, Ithaca, NY 14853, USA*
[5]*National High Magnetic Field Laboratory, Florida State University, Tallahassee, FL 32310, USA*
[6]*Advanced Photon Source, Argonne National Laboratory, Argonne, IL 60439, USA*
(Dated: November 28, 2020)

EXPERIMENTAL METHODS

A. Samples

Our study was conducted on multiple single crystals of $Ta_4Pd_3Te_{16}$ that were grown using a self-flux with excess tellurium at T up to 1000°C. High-resolution single-crystal X-ray diffraction confirmed the quality of the crystals and their orientations. The same batch of samples has been used in previous thermodynamic and transport studies [1]. We refer readers to Ref. [1] for details of crystal characterizations.

To further confirm the high quality of our single crystals, we also measured the X-ray diffraction pattern of a typical single crystal sample, using a RIGAKU Miniflex 6G powder X-ray diffractometer, as shown in Fig. S1(a). The full width at half-maximum is 0.07° for the (-309) peak, which is limited by the resolution of our diffractometer. The same result is also obtained from our single crystal X-ray diffraction measurements using a Bruker X8-APEXII diffractometer. The width of the Bragg peaks is comparable to that reported in Ref. [2], confirming the high quality of our single crystals.

The rocking curves for single crystal samples used in our ambient-P X-ray diffraction measurements at CHESS and high-P X-ray diffraction measurements at APS are shown in Fig. S1(b) and S1(c), respectively. The high quality of our single crystals is further confirmed by the sharp Bragg peaks (mosaic spread $\sim 0.1°$) in the rocking curves.

B. de Haas-van Alphen quantum oscillation

The dHvA quantum oscillation measurements were performed in a ^{3}He cryostat and an 18 T superconducting magnet at the National High Magnetic Field Laboratory (NHMFL) using piezo-resistive cantilevers and samples with typical dimensions $\sim 60 \times 60 \times 30 \ \mu m^3$. The angle between the applied magnetic field and the crystalline **c** axis is $\sim 15°$.

C. Synchrotron X-ray diffraction at ambient pressure

The ambient-pressure high-dynamic-range diffraction maps were collected at the A2 beamline at Cornell High Energy Synchrotron Source (CHESS), using 19.37 keV X-rays and a fast photon-counting area detector. A needle-shaped single crystal sample was affixed at one end to a copper post, which was subsequently mounted in transmission geometry inside a closed-cycle cryostat with a base T of 3.5 K.

D. Synchrotron X-ray diffraction at high pressure

For high pressure measurements, single crystals of $Ta_4Pd_3Te_{16}$ are cut into bar shapes with typical dimensions $\sim 100 \times 60 \times 30 \ \mu m^3$ (length $\times$ width $\times$ thickness). Sample qualities were then checked using single-crystal X-ray diffraction, and the best samples were selected and loaded into a 800-μm-culet diamond anvil cell using 4:1

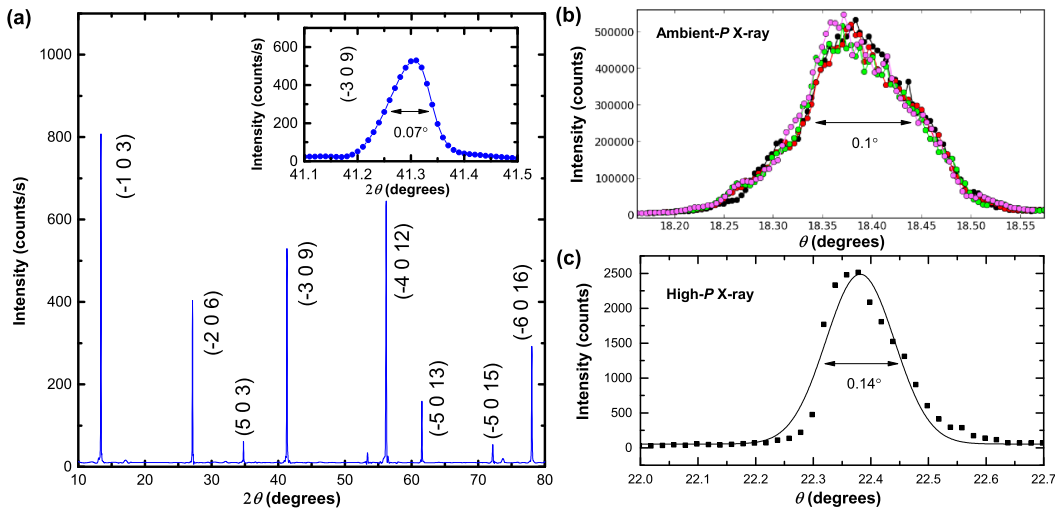FIG. S1. (a) X-ray diffraction pattern of Ta$_4$Pd$_3$Te$_{16}$ single crystal sample obtained from a RIGAKU Miniflex 6G powder X-ray diffractometer. Inset: the (-309) reflection with a resolution-limited width 0.07°. (b) X-ray rocking curve of the (040) peak for the ambient-P X-ray diffraction experiment at CHESS. The four traces are repeated measurements throughout the experiment. (c) X-ray rocking curve of the (60-2) peak for the high-P diffraction measurement at APS. The sharp peaks (i.e. mosaic spread $\sim 0.1°$) in the rocking curves indicate the high-quality of our single crystal samples. A shoulder-like feature in both rocking curves, likely from the twin domains inevitable in monoclinic single crystals, does not affect our CDW diffraction measurements, because the CDW peak width is two orders of magnitude larger than the resolution-limited Bragg peaks, as discussed in the main text.

Methanol:Ethanol as the hydrostatic pressure medium and a polycrystalline gold foil as the manometer. The value of the pressure was averaged over three to four measurements, and the uncertainty of the pressure reading is ~ 0.1 GPa in our experiment range of 0 to 0.35 GPa. In-situ pressure tuning was enabled by a helium gas membrane. The high-pressure experiments were conducted at the 4-ID-D beamline at the Advanced Photon Source (APS), using 19.5 keV X-rays, a six-circle diffractometer, and a Sumitomo closed-cycle cryostat with a base T of 4 K.

dHvA QUANTUM OSCILLATION RESULTS

In chargen density wave (CDW) systems where the structure is modulated, the unit cell is enlarged and the bands backfold onto one another. If the bands happen to be crossing the Fermi surface (FS) at the modulated wavevector, the FS is reconstructed such that a gap emerges. This change in FS topology can often be detected in quantum oscillation (QO) measurements, if the FS is closed. We have therefore conducted magnetic torque measurements to study the dHvA oscillations, and the background-subtracted results are shown in Fig. S2(b). Here, the fast Fourier transform taken for the field window of 5.4 T and 18 T reveals two frequencies F_1 and F_2 [Fig. S2(c)]. The fitting of the Lifshitz-Kosevich temperature damping factor $R_T = (K\mu T/B)/\sinh{(K\mu T/B)}$ results in an effective mass of $\mu_{F1} = (0.108 \pm 0.005)m_e$ and $\mu_{F2} = (0.127 \pm 0.008)m_e$, where m_e is the bare electron mass and $K = 14.7$ T/K. The results are in rough agreement with the lowest two frequencies reported in Ref. [1], and in both cases, no FS reconstruction is observed as T is tuned through $T_{\mathrm{CDW}} \sim 16$ K. To explain the observed QO results [1], a scenario was postulated in which an incommensurate CDW, already appearing at higher T, undergoes an incommensurate-to-commensurate lock-in transition at ~ 20 K. However, as we show below, our X-ray results reveal an incommensurate CDW at T down to 3.5 K. The QO results therefore cannot be explained by a lock-in transition at T_{CDW}. Instead, this aspect of the CDW seems similar to that of NbSe$_2$, where the CDW gap opens only at select points on one band of the multi-orbital FS and the change in the topology of the FS might be very subtle [3].
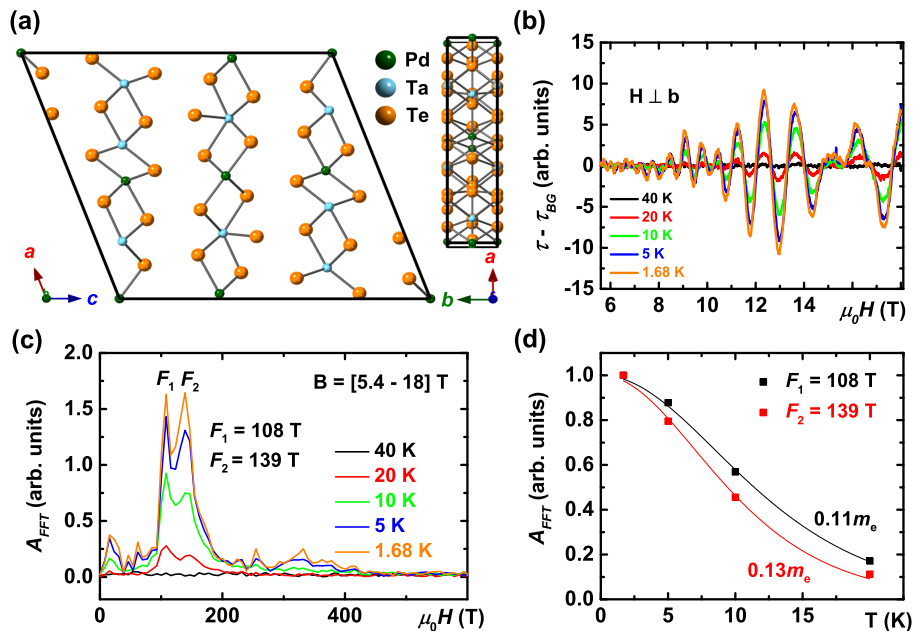
FIG. S2. (a) Crystal structure of $Ta_4Pd_3Te_{16}$ along the [010] and [-103] directions in one unit cell. Chains along **b** comprise planes perpendicular to **c**. (b) dHvA oscillation data with polynomial background subtracted at various temperatures measured in an 18 T superconducting magnet. (c) Fourier transform of the data from (b) over a field window of 5.4 to 18 T. (d) Lifshitz-Kosevich fitting of the effective mass.

CDW IN $Ta_4Pd_3Te_{16}$

A. CDW projections

The structure of $Ta_4Pd_3Te_{16}$ and its relation to its CDW is shown in Fig. S3. The projection of the CDW into the **a-c** plane has a period of 5 unit cells along **a** and a period of 10/3 unit cells along **c**. As there are 3 chains per unit cell along **c**, the length of $10c/3$ corresponds to a period of 10 chains in this direction. **Q1** and **Q2** CDWs both project in the same way in the **a-c** plane.

STM accesses the (-1 0 3) clevage plane, containing the perpendicular vectors **a*** and **b** [4]. In the **a*** direction the crystal structure repeats every $a_\perp = 49.8$ Å. The projection of the CDWs along **a*** give a period of $1.13a_\perp$ distortion. In the **b** direction, both CDW wavevectors give a period of $b/0.21 \approx 4.76b$ distortion. While the periodicities seen by X-rays are therefore incommensurate in both the **a*** and **b** directions, the resulting CDW patterns would be expected to lock into commensurate structures locally, with phase slips to allow for the globally incommensurate patterns [5, 6]. This is expected both in the bulk and on the surface; however, surface effects could plausibly fully stabilize the commensurate CDW, removing the phase slips. The CDW would normally lock into a nearby rational period, with lower periods expected to be favored. STM would therefore be likely to see a CDW with period of either 4 or 5 along **b**, and period 1 (*i.e.* no CDW) or 2 along **a***. Carrying out the Fourier transform of the STM image given in Ref. [4], the resulting diffraction peaks can be indexed with $\mathbf{a}^*_\perp \pm \mathbf{b}^*/4$, where $\mathbf{a}^*_\perp$ is a vector along **a*** of length $2\pi/a_\perp$. The surface CDW is therefore of period one along **a*** and four along **b**, and is consistent with our X-ray measurements.

Our results also shed light on the resistivity anomaly observed in the transport study [1]. At $T_{CDW} \sim 16$ K, it was reported [1] that an increase of resistivity was observed along the **a*** direction, while far less significant increases were seen along the **b** and **c** directions. This is despite STM reporting a charge modulation along **b**. Our X-ray results show a commensurate structure in the **a-c** plane, with a large component along **a***. Therefore a resistivity bump along that direction comes as no surprise. The CDW component along **b** is incommensurate with the lattice (in the bulk of the crystal, if not at the surface), which might explain the lack of a resistivity feature associated with the CDW in this direction [7].
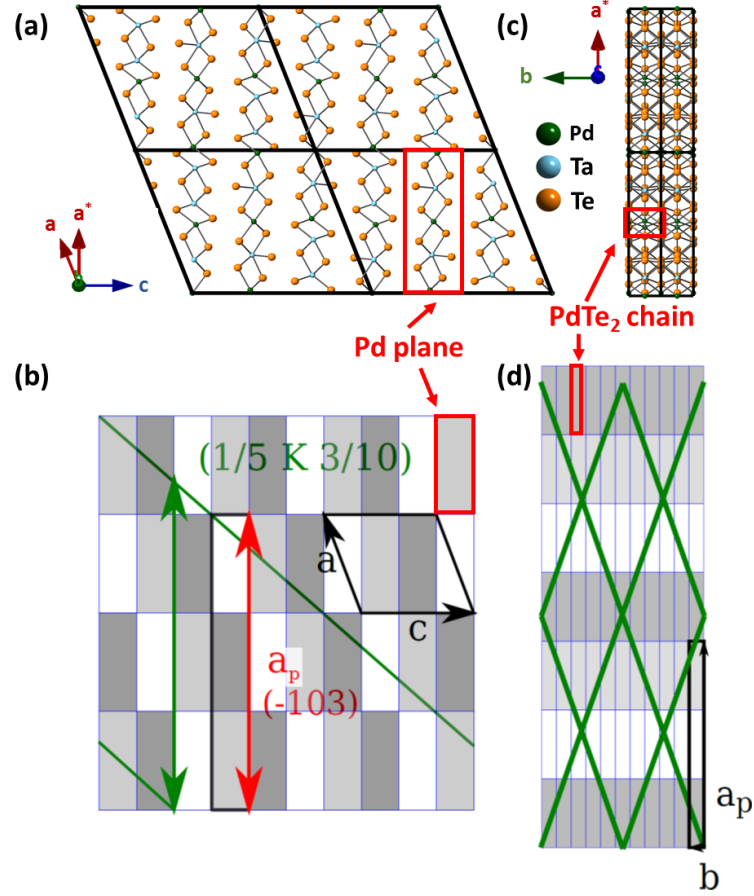
FIG. S3. Schematic representation of the unit cell of $Ta_4Pd_3Te_{16}$ and the CDW projection onto the unit cells: (a-b) in the **a**-**c** plane, (c-d) the **a***-**b** plane, where $\mathbf{a^*}(\|\mathbf{a_p}})$ is perpendicular to **b** and **c**. Each tile in (b) and (d) corresponds to one of the three Pd planes (chains) within one unit cell in (a) and (c), as represented by the red box. The three shades of the tiles correspond to the three different planes (chains). The vector $\mathbf{a_p}$ is along $\mathbf{a^*}$ and defined by the length of the three tiles. The natural cleavage plane (-1 0 3), investigated by STM (24), contains the perpendicular vectors $\mathbf{a^*}$ ($\|\mathbf{a_p}$) and **b**. In the $\mathbf{a^*}$ direction the crystal structure repeats every $a_\perp$ (= 49.8 Å). The projection of the CDWs along $\mathbf{a^*}$ give a period $1.13a_\perp$ distortion, as indicated by the double-sided green arrow. In (b) and (d), CDW planes are shown in green solid lines: in (b), the CDW projection has a period of $1.13a_\perp$ along $\mathbf{a^*}$ and 10/3 along **c**; while in (d), the CDW projection has a period $1.13a_\perp$ along $\mathbf{a^*}$, and 4.76 along **b**. Note that the two CDW wavevectors ($\mathbf{Q1}$ and $\mathbf{Q2}$) have a π-rotational symmetry about the **b**-axis, a crystal symmetry, as seen in (d).

B. CDW correlation length

In X-ray diffraction measurements, the measured peak shape is determined by the convolution of the intrinsic shape of the peak and the shape of the instrumental resolution function. The latter is usually very sharp for a Synchrotron x-ray diffraction measurement, and its width can be estimated from the width of the lattice Bragg peak of the high quality single crystal. Here, the width of the Bragg peak is two orders of magnitude smaller than the CDW peak in $Ta_4Pd_3Te_{16}$. Therefore, the instrumental resolution function does not contribute to the width of the observed CDW peak.

The CDW correlation length ξ_{CDW} is then determined from the full width at half maximum (FWHM) of the Lorentzian fit of the CDW peak. At low T, FWHM ~ 0.01 r.l.u. $= 0.01*2\pi/b = 0.0168$ Å^{-1}, along $\mathbf{q_k}$ [Fig. 3(c)]. Therefore, $\xi_{CDW} = 2/\text{FWHM} \sim 119$ Å. The error in the estimation of the CDW correlation length is determined by the error in the FWHM of the Lorentzian fit. At 3.5 K, 0 GPa, for example, FWHM = 0.013 r.l.u. and its error $\Delta\text{FWHM} = 0.001$ r.l.u. A quick estimation gives the error of CDW correlation length $\Delta\xi_{CDW} \sim 9$ Å.
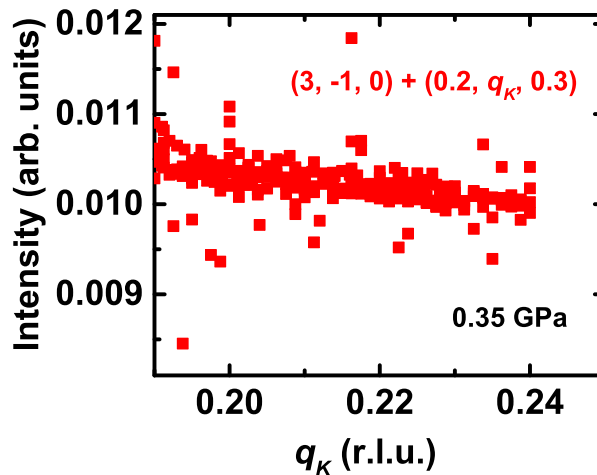
FIG. S4. Raw data (without any background subtraction) of eight scans of X-ray diffraction intensity near the expected CDW wavevector $\mathbf{Q2}$ at our base $T = 4.3$ K and $P = 0.35$ GPa. Sample alignment was checked twice in between these eight scans to ensure the accuracy of the result. No CDW peak was observed within experimental resolution. Thus we consider $T_{\mathrm{CDW}} \to 0$ at $P = 0.35$ GPa.

C. Pressure points in the high-P Synchrotron X-ray diffraction measurements

A common experimental challenge for high-P Synchrotron X-ray diffraction measurements is the precise pressure control in diamond anvil cells (DAC) at low temperatures. This is especially true for the low-pressure limit, which is the regime of interest in our study on $\mathrm{Ta_4Pd_3Te_{16}}$.

To achieve the lowest pressure possible, we sealed the pressure cell with pressure medium but did not apply any pressure, so that the $P = 0$ at room temperature. After cooling down, the pressure increases to ~ 0.2 GPa. In fact, a pressure drift ($0.1 \sim 0.2$ GPa or more, depending on the type of the cell and pressure medium) is usually expected when T is changed from 300 K to low T. Therefore, we were not able to obtain any lower pressure point.

To increase the pressure at low temperatures, we used a helium gas membrane to apply a small pressure to the DAC and reached ~ 0.35 GPa. As shown in Fig. S4, we repeated eight scans near the expected CDW wavevector $\mathbf{Q2}$ at base temperature $T = 4.3$ K, but did not find any CDW peak. We also checked sample alignment twice in between these scans to ensure experimental accuracy. Since no CDW is seen at the lowest temperature of our measurement, we consider this as a null data point with $T_{\mathrm{CDW}} \sim 0$ at $P = 0.35$ GPa.

CDWS IN PROTOTYPICAL CDW MATERIALS

A. CDW structures

Insights on the CDW in $\mathrm{Ta_4Pd_3Te_{16}}$ can also be obtained in comparison with prototypical Q1D and Q2D CDW materials.

The case of $\mathrm{NbSe_3}$ is representative of the transition metal trichalcogenides, and is the prototypical example of a Q1D Peierls CDW material. It hosts two CDWs with wavevectors $\mathbf{Q1}$=(0 0.241 0), $\mathbf{Q2}$=(1/2 0.260 1/2) [8]. The $\mathbf{Q2}$ CDW is known to develop at a higher temperature on the surface of the material than in the bulk, with the surface order believed to develop in a Kosterlitz–Thouless transition [9]. STM sees a locally commensurate CDW structure on the surface, with periodic phase slips allowing for an incommensurate average wavevector [10]. These facts align with our suggestions regarding discrepancies between the surface and bulk probes of the CDW order in $\mathrm{Ta_4Pd_3Te_{16}}$. However, unlike $\mathrm{Ta_4Pd_3Te_{16}}$, the two CDWs in $\mathrm{NbSe_3}$ are not related by a lattice symmetry, and develop at different temperatures [11]. They are therefore two independent CDWs, with independent order parameters, rather than a checkerboard CDW.

Another class of Q1D CDW materials is the rare-earth tri-tellurides $R\mathrm{Te_3}$ (R =Sm, Gd, Tb, Dy, Ho, Er, Tm). The crystal structure of these materials is weakly orthorhombic, but is very close to the monoclinic structure of $\mathrm{Ta_4Pd_3Te_{16}}$ [12]. All of these compounds develop incommensurate CDWs with $\mathbf{Q1} \approx 2\mathbf{c}^*/7$; the heavier elements

(R =Dy, Ho, Er, Tm) also develop a second incommensurate CDW, with $\mathbf{Q2} \approx \mathbf{a}^*/3$. However, as in the trichalco-genides, these two CDWs develop at different temperatures, and are not related by lattice symmetries.

For Q2D CDW materials, the transition metal dichalcogenides (TMDC) $2H$-NbSe$_2$, $2H$-TaSe$_2$, and $1T$-TaS$_2$ [13, 14] are typical examples. The $2H$ materials have a hexagonal crystal structure, and the $1T$ a trigonal structure. In $2H$-NbSe$_2$, for instance, a checkerboard CDW develops within the hexagonal Q2D planes, with three incommensurate CDW wavevectors developing at the same temperature and related by the C_6 lattice symmetry [15]. In all these cases, the CDW which develops does so entirely within the Q2D planes. An exception is $1T$-TiSe$_2$, a Q2D TMDC which develops a three-dimensional commensurate $2 \times 2 \times 2$ CDW, although even in this case the CDW wavevector fits to the Q2D planes, with order also between the planes [16].

The closest relative of the CDW in Ta$_4$Pd$_3$Te$_{16}$ is perhaps that in $1T$-VSe$_2$, a TMDC with a mixed Q2D and 3D character [17]. This material develops a CDW with commensurate period-4 components within the Q2D planes, but an incommensurate component out-of-plane [17]. The three CDW wavevectors are related by a C_3 lattice symmetry, and develop at the same temperature. The incommensurate wavevector in VSe$_2$ evolves with temperature but never locks into the lattice. The CDW has no corresponding FSN structure, as demonstrated by a lack of divergence in the electronic susceptibility (Lindhard response function) [18], and ARPES sees no obvious disruption of the FS as the CDW develops [19].

We also made a simple estimate of the Lindhard function in Ta$_4$Pd$_3$Te$_{16}$ using existing DFT data, and found no divergences [1, 20]. This again suggests a more complicated origin of the CDW than simple FSN [21, 22]. In general, FSN is not the natural assumption when CDWs are encountered in dimensions higher than one: while a single CDW wavevector can gap out the entire FS in 1D, in dimensions higher than one the wavevectors would need to connect large parts of the FS. It seems reasonable to surmise that the CDW mechanism in Ta$_4$Pd$_3$Te$_{16}$ is the same as that in the other $D > 1$ CDW systems: TMDCs $2H$-NbSe$_2$ [23] and $1T$-VSe$_2$ [18], in which the CDWs are known to originate from a structured electron-phonon coupling dependent on both the ingoing and outgoing electron momenta and the orbital content of the bands scattered between [3].

B. $T - P$ phase diagrams

As noted in the main text, the effect of the pressure on T_{CDW} might reveal how Q1D the system really is. Here we show a thorough survey of the T-P phase diagrams of prototypical CDW materials and their comparisons with Ta$_4$Pd$_3$Te$_{16}$ (See Fig. S5).

Amongst the materials reported as Q1D, (TaSe$_4$)$_2$I [31, 32] shows an initial increase in T_{CDW} with pressure, and monoclinic TaS$_3$ appears to behave similarly, but the superconducting dome is not reached by the highest pressures of around 30GPa. On the other hand, o-TaS$_3$ [31, 32], ZrTe$_3$, GdTe$_3$, TbTe$_3$, DyTe$_3$ [33], and NbSe$_3$ [31, 32] show a decrease in T_{CDW} with pressure. Despite the resistivity anisotropies of these materials indicating a Q1D nature, the T_{CDW} behavior fits more closely to 3D materials.

For Q2D materials, CDWs are suppressed under pressure in most cases, and a competitive interplay of the CDW and SC is often observed [34, 35], as discussed in the main text. CDWs are also seen in 3D materials such as R$_3$T$_4$X$_{13}$ featuring cubic symmetry. Application of chemical or physical pressure also suppresses T_{CDW} to zero in this case [37, 38]. However, we do note there is some exception. Recent work reports that the Q2D-3D hybrid $1T$-VSe$_2$ shows an unexpected increase in T_{CDW} with pressure, followed by an abrupt suppression of the CDW and development of superconductivity (SC) above around 15 GPa [36]. However, these estimates are based on tracking the minimum in $\mathrm{d}\rho/\mathrm{d}T$ from resistivity (ρ) measurements, and the true relation between this quantity and the CDW state remains to be identified.
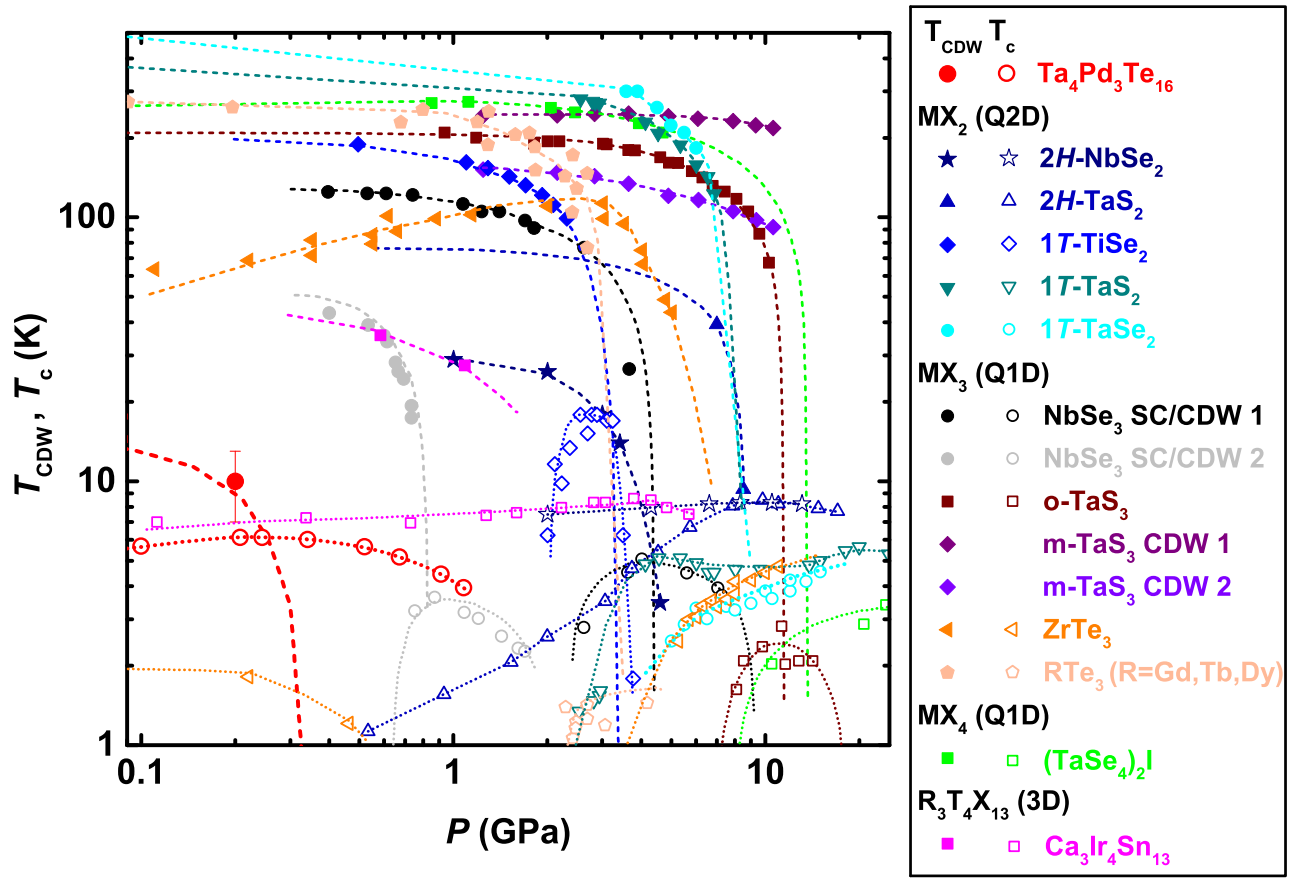
FIG. S5. Phase diagram of prototypical compounds, as a function of T and P in logarithmic scales, showing T_{CDW} (solid symbols) and T_c (empty symbols). The logarithmic scales are necessary to show the vastly different scales in these systems, though our data poinst at $P = 0$ and $T_{\mathrm{CDW}} \sim 0$ become hidden. Neverthelss, the CDW phase boundary for $Ta_4Pd_3Te_{16}$, determined from our X-ray measurements at 0, 0.2, and 0.35 GPa [Fig. 3(d)], is shown as the red dashed line along with T_c values from Ref. [24]. Other compounds: $2H$-NbSe$_2$ (Ref. [25], and unplished data from Sven Friedemann's group), $2H$-TaS$_2$ [26, 27]; $1T$-TaS$_2$ [28]; $1T$-TaSe$_2$ [29]; $1T$-TiSe$_2$ [30]; (TaSe$_4$)$_2$I [31, 32]; o-TaS$_3$ and m-TaS$_3$ [31, 32]; ZrTe$_3$, GdTe$_3$, TbTe$_3$, DyTe$_3$ [33]; NbSe$_3$ [31, 32]; Ca$_3$Ir$_4$Sn$_{13}$ [37, 38].

[1] T. Helm *et al.*, *Thermodynamic anomaly above the superconducting critical temperature in the quasi-one-dimensional superconductor $Ta_4Pd_3Te_{16}$.* Phys. Rev. B **95**, 075121 (2017).

[2] W.-H. Jiao, Z. T. Tang, Y. L. Sun, Y. Liu, Q. Tao, C.-M. Feng, Y.-W. Zeng, Z.-A. Xu, and G.-H. Cao, *Superconductivity in a layered $Ta_4Pd_3Te_{16}$ with $PdTe_2$ chains.* J. Am. Chem. Soc. **136**, 1284 (2014).

[3] F. Flicker and J. van Wezel, *Charge order in $NbSe_2$.* Phys. Rev. B **94**, 235135 (2016).

[4] Q. Fan *et al.*, *Scanning tunneling microscopy study of superconductivity, magnetic vortices, and possible charge-density wave in $Ta_4Pd_3Te_{16}$.* Phys. Rev. B **91**, 104506 (2015).

[5] W. L. McMillan, *Theory of discommensurations and the commensurate-incommensurate charge-density-wave phase transition.* Phys. Rev. B **14**, 1496 (1976).

[6] F. Flicker and Jasper van Wezel, *Quasiperiodicity and 2D topology in 1D charge-ordered materials.* Europhysics Letters **111**, 37008 (2015).

[7] P. Monceau, *Electronic crystals: an experimental overview.* Adv. Phys. **61**, 325 (2012).

[8] R. M. Fleming, D. E. Moncton, and D. B. McWhan, *X-ray scattering and electric field studies of the sliding mode conductor $NbSe_3$.* Phys. Rev. B **18**, 5560 (1978).

[9] C. Brun, Z. Z. Wang, P. Monceau, and S. Brazovskii, *Surface Charge Density Wave Phase Transition in $NbSe_3$.* Phys. Rev. Lett. **104** 256403 (2010).

[10] S. Brazovskii, C. Brun, Z. Z. Wang, and P. Monceau, *Scanning-tunneling microscope imaging of single-electron solitons in a material with incommensurate charge-density waves.* Phys. Rev. Lett. **108** 096801 (2012).

[11] J. Chaussy, P. Haen, J.-C. Lasjaunias, P. Monceau, G. Waysand, A. Waintal, A. Meerschaut, P. Molinié, and J. Rouxel, *Phase transitions in $NbSe_3$.* Solid State Commun. **20**, 759 (1976).

[12] N. Ru, C. L. Condron, G. Y. Margulis, K. Y. Shin, J. Laverock, S. B. Dugdale, M. F. Toney, and I. R. Fisher, *Effect of chemical pressure on the charge density wave transition in rare-earth tritellurides RTe_3.* Phys. Rev. B **77**, 035114 (2008).

[13] B. Giambattista, C. Slough, W. McNairy, and R. Coleman, *Scanning tunneling microscopy of atoms and charge-density waves in $1T$-TaS_2, $1T$-$TaSe_2$, and $1T$-VSe_2.* Phys. Rev. B **41**, 10082 (1990).

[14] Y. Feng, J. van Wezel, J. Wang, F. Flicker, D. M. Silevitch, P. B. Littlewood, and T. F. Rosenbaum, *Itinerant density wave instabilities at classical and quantum critical points.* Nat. Phys. **11**, 865 (2015).

[15] J. A. Wilson, F. J. Di Salvo, and S. Mahajan, *Charge-density waves in metallic, layered, transition-metal dichalcogenides.* Phys. Rev. Lett. **32**, 882-885 (1974).

[16] A. Kogar, M. S. Rak, S. Vig, A. A. Husain, F. Flicker, Y. I. Joe, L. Venema, G. J. MacDougall, T. C. Chiang, E. Fradkin, J. van Wezel, and P. Abbamonte, *Signatures of exciton condensation in a transition metal dichalcogenide.* Science 358, 1314-1317 (2017).

[17] K. Tsutsumi, *X-ray-diffraction study of the periodic lattice distortion associated with a charge-density wave in $1T$-VSe_2.* Phys. Rev. B **26**, 5756 (1982).

[18] J. Henke, J. Laverock, F. Flicker, and J. van Wezel, *Charge order from structured coupling in VSe_2.* arXiv:1911.11112 (25 November 2019).

[19] K. Terashima, T. Sato, H. Komatsu, T. Takahashi, N. Maeda, and K. Hayashi, *Charge-density wave transition of $1T$-VSe_2 studied by angle-resolved photoemission spectroscopy.* Phys. Rev. B **68**, 155108 (2003).

[20] D. J. Singh, *Multiband superconductivity of $Ta_4Pd_3Te_{16}$ from Te p states.* Phys. Rev. B **90**, 144501 (2014).

[21] M. D. Johannes and I. I. Mazin, *Fermi surface nesting and the origin of charge density waves in metals.* Phys. Rev. B **77**, 165135 (2008).

[22] X. Zhu, Y. Cao, J. Zhang, E. W. Plummer, and J. Guo, *Classification of charge density waves based on their nature.* Proc. Natl. Acad. Sci. U.S.A. **112**, 2367 (2015).

[23] F. Flicker and J. van Wezel, *Charge order from orbital-dependent coupling evidenced by $NbSe_2$.* Nat. Commun. **6**, 7034 (2015).

[24] N. H. Jo, L. Xiang, U. S. Kaluarachchi, M. Masters, K. Neilson, S. S. Downing, P. C. Canfield, and S. L. Bud'ko, *Pressure induced change in the electronic state of $Ta_4Pd_3Te_{16}$.* Phys. Rev. B **95**, 134516 (2017).

[25] M. Leroux, I. Errea, M. Le Tacon, S.-M. Souliou, G. Garbarino, L. Cario, A. Bosak, F. Mauri, M. Calandra, and P. Rodière, Strong anharmonicity induces quantum melting of charge density wave in $2H$-$NbSe_2$ under pressure. Phys. Rev. B **92**, 140303(R) (2015).

[26] R. Grasset, Y. Gallais, A. Sacuto, M. Cazayous, S. Mañas-Valero, E. Coronado, and M.-A. Méasson, Pressure-Induced Collapse of the Charge Density Wave and Higgs Mode Visibility in $2H$-TaS_2. Phys. Rev. Lett. **122** 127001 (2019).

[27] D. C. Freitas *et al.*, Strong enhancement of superconductivity at high pressures within the charge-density-wave states of $2H$-TaS_2 and $2H$-$TaSe_2$. Phys. Rev. B **93** 184512 (2016).

[28] B. Sipos, A. F. Kusmartseva, A. Akrap, H. Berger, L. Forr, and E. Tutis, From Mott state to superconductivity in $1T$-TaS_2. Nature Mater. **7**, 960 (2008).

[29] B. Wang *et al.*, Pressure-induced bulk superconductivity in a layered transition-metal dichalcogenide $1T$-tantalum selenium. Phys. Rev. B **95**, 220501(R) (2017).

[30] A. F. Kusmartseva, B. Sipos, H. Berger, L. Forró, and E. Tutič, Pressure induced superconductivity in pristine $1T$-$TiSe_2$. Phys. Rev. Lett. **103**, 236401 (2009).

[31] M. Núñez-Regueiro, J.-M. Mignot, and D. Castello, *Superconductivity at High Pressure in $NbSe_3$.* Europhys. Lett. **18**, 53 (1992).

[32] M. Núñez-Regueiro *et al.*, *Superconductivity under pressure in linear chalcogenides.* Synthetic Metals **55-57**, 2653 (1993).

[33] D. A. Zocco *et al.*, *Pressure dependence of the charge-density-wave and superconducting states in $GdTe_3$, $TbTe_3$, and $DyTe_3$.* Phys. Rev. B **91**, 205114 (2015).

[34] A. Majumdar *et al.*, *Interplay of charge density wave and multiband superconductivity in layered quasi-two-dimensional materials: The case of $2H$-NbS_2 and $2H$-$NbSe_2$.* Phys. Rev. Materials **4** 084005 (2020).

[35] Y. Kvashnin, D. VanGennep, M. Mito, S. A. Medvedev, R. Thiyagarajan, O. Karis, A. N. Vasiliev, O. Eriksson, and M. Abdel-Hafiez, *Coexistence of Superconductivity and Charge Density Waves in Tantalum Disulfide: Experiment and Theory* Phys. Rev. Lett. **125** 186401 (2020).

[36] S. Sahoo, U. Dutta, L. Harnagea, A.K. Sood, S. Karmakar, *Pressure-induced suppression of charge density wave and emergence of Superconductivity in $1T$-VSe_2.* Phys. Rev. B **101**, 014514 (2020).

[37] L. E. Klintberg, S. K. Goh, P. L. Alireza, P. J. Saines, D. A. Tompsett, P. W. Logg, J. Yang, B. Chen, K. Yoshimura, and F. M. Grosche *Pressure- and composition-induced structural quantum phase transition in the cubic superconductor $(Sr,Ca)_3Ir_4Sn_{13}$.* Phys. Rev. Lett. **109**, 237008 (2012).

[38] S. K. Goh, L. E. Klintberg, P. L. Alireza, D. A. Tompsett, J. Yang, B. Chen, K. Yoshimura, and F. M. Grosche *Enhancement of the superconducting transition temperature with hydrostatic pressure in $Ca_3Ir_4Sn_{13}$ single crystals.* arXiv:1105.3941 (19 May 2011).